Double-threshold technique for achieving denoising in compressive imaging applications

Chao Wang (王 超)[1,2,3], Xuri Yao (姚旭日)[3,*], and Qing Zhao (赵 清)[1]

[1]*Center for Quantum Technology Research, School of Physics, Beijing Institute of Technology, Beijing 100081, China*
[2]*China Academy of Engineering Physics, Mianyang 621900, China*
[3]*Key Laboratory of Electronics and Information Technology for Space Systems, National Space Science Center,*
Chinese Academy of Sciences, Beijing 100190, China
*Corresponding author: yaoxuri@aliyun.com

Received September 15, 2017; accepted September 22, 2017; posted online November 3, 2017

Single-pixel cameras, which employ either structured illumination or image modulation and compressive sensing algorithms, provide an alternative approach to imaging in scenarios where the use of a detector array is restricted or difficult because of cost or technological constraints. In this work, we present a robust imaging method based on compressive imaging that sets two thresholds to select the measurement data for image reconstruction. The experimental and numerical simulation results show that the proposed double-threshold compressive imaging protocol provides better image quality than previous compressive imaging schemes. Faster imaging speeds can be attained using this scheme because it requires less data storage space and computing time. Thus, this denoising method offers a very effective approach to promote the implementation of compressive imaging in real-time practical applications.

OCIS codes: 110.0110, 110.2990, 100.3010.
doi: 10.3788/COL201715.121101.

Classical image formation is most commonly realized by creating an image of a scene onto a detector array. In scenarios where using a detector array is restricted or difficult because of cost or technological constraints, alternative imaging approaches are required. In several imaging devices, scanning methods serve as the method of choice, although these methods have the disadvantage of the acquisition times being linearly proportional to the spatial resolution. Compressive imaging (CI)[1] provides the promising option of using a single-pixel detector to facilitate the structured detection of an image or the structured illumination onto a scene to deduce an image. CI also has the advantage of under-sampling. In compressive sensing (CS)[2,3], which relies on the empirical observation that many types of signals or images are sparse in the appropriate basis, an image can be recovered from fewer measurements than those required according to the Nyquist–Shannon criterion. Because CI has the advantages of compressive detection and a simple experimental configuration, it has attracted wide attention in many fields, such as infrared imaging[4,5], three-dimensional (3D) imaging[6–9], fluorescence microscopy[10,11], spectroscopic imaging[12,13], super-resolution domain imaging[14–17], and terahertz (THz) imaging[18].

When using the CI approach, it is essential to maintain the high quality of the reconstructed images. Generally, to implement a CI system, a series of 0/1 binary transmission masks realized by a digital micromirror device (DMD) are applied to carry out light intensity modulation. However, the binary 0/1 matrix is not the best choice for CI because it does not satisfy the restricted isometry property condition, which plays a major role in ensuring CS robustness.

To address this problem, the $-1/1$ binary matrix with a zero mean is employed in CI[19–21]. Because only non-negative matrices can be physically displayed by the DMD, the $-1/1$ binary matrix is realized by displaying a 0/1 pattern immediately followed by its inverse or by detecting the light reflected in both the directions of the DMD. Alternative approaches for increasing the signal-to-noise ratio (SNR) of a reconstructed image are the use of Hadamard matrices[22] or the use of sinusoidal patterns to retrieve its Fourier spectrum[23]. The CI system is very similar to computational ghost imaging[24–26], which also uses the knowledge of structured illumination patterns and single-pixel detector signals to reduce an image. In ghost imaging, some threshold strategies[27–30] have been proposed to offer a better SNR and improved visibility by computing certain patterns selected by the thresholds.

In our previous work[31], a threshold configuration was employed to improve the image quality in CI. In this Letter, we present an approach that utilizes two thresholds to reduce the noise in CI. We select low-noise, large-fluctuation signals for the calculation based on this approach. We show that by using this method image quality can be effectively improved, while saving both computational time and storage space. This threshold algorithm does not require any modification to the existing experimental apparatus. The experimental results indicate that this threshold strategy can provide better image quality and a higher SNR than previous complementary CI schemes. Because of these advantages, the proposed double-threshold method is expected to be useful in real-time practical applications.

We use an n-dimensional vector $O(x)$ to denote the object. Suppose that there exists a transform matrix Ψ to the sparse basis, such that $O(x) = \Psi \cdot O'(x')$, where $O'(x')$ is sparse. Generally, many natural signals, such as images, are sparse in the appropriate basis. In CS, an $m \times n$ matrix A is used to describe the measuring device $m < n$, and the measurement process can be formulated as

$$y = A\Psi O'(x') + e, \tag{1}$$

where y is an m-dimensional observation vector, and e is the noise. In this study, the complementary measurement method is adopted[19–21]. Thus, A is a $-1/1$ binary matrix with a zero mean. As mentioned above, during the implementation, the $-1/1$ binary matrix is realized by displaying a 0/1 binary matrix followed by its inverse, and two intensity signals S_j^+ and S_j^- are obtained. The element in the observation vector y is obtained from the difference between these two intensity signals:

$$y_j = S_j^+ - S_j^-. \tag{2}$$

Because $m < n$, the observation vector y does not specify a unique $O(x)$. In CS, the following optimization problem is solved to reconstruct the object information:

$$\hat{O}'(x') = \arg\min\left\{ ||A \cdot \Psi \cdot O'(x') - y||_2^2 \right.$$
$$\left. - \tau||O'(x')||_1 \right\},$$
$$\hat{O}(x) = \Psi \cdot \hat{O}'(x'), \tag{3}$$

where $\hat{O}(x)$ is the reconstructed image, and τ is a constant scalar, weighing the relative strength of the two terms.

We employ a threshold T_1 to select the measurements,

$$y_{T_1} = \{|y| > T_1\}. \tag{4}$$

The values in y represent the comparability of the object and the random binary patterns. The larger the value of $|y|$, the greater the degree of correlation is between the object and the random binary pattern[30].

The sum of the two intensity signals of the complementary binary patterns

$$S_j = S_j^+ + S_j^-, \tag{5}$$

should be a constant in the absence of noise. We employ another threshold T_2 to select the measurements:

$$\{y_{T_2}||S_j - \bar{S}| < T_2\}, \tag{6}$$

where $\bar{S} = (1/m)\sum_{j=1}^{m} S_j$ is the mean of the sum of the two intensity signals.

The double thresholds are utilized jointly in this work. y_T is the intersection between y_{T_1} and y_{T_2};

$$y_T = \{|y| > T_1\}, \{y_T||S_j - \bar{S}| < T_2\}. \tag{7}$$

The measurement vector after reduction is used to reconstruct the object. Accordingly, the rows in matrix A are reduced, and A_t is the matrix after reduction. The values of these double thresholds will be discussed later.

A schematic diagram of the experimental apparatus is shown in Fig. 1(a). A stabilized tungsten-halogen light source (SLS201, Thorlabs Inc.), combined with a collimated lens, is used to illuminate the object, which is the Group 2, Element 3 portion of the standard U.S. Air Force resolution target. A narrow-band filter of 640 nm with a full width at half-maximum of 10 nm is positioned behind the object. The object is imaged onto the DMD using an achromatic imaging lens ($\Phi = 25.4$ mm, $f = 50.4$ mm). The DMD consists of a 1024×768 array of independently configurable mirrors, and the size of each mirror is 13.68 μm × 13.68 μm. Each mirror can be shifted between two positions oriented at $+12°$ (1) or $-12°$ (0) with respect to the surface of the DMD. The light reflected by the micromirrors oriented at $+12°$ is focused onto a CCD (1620M, IMPERX Inc.) by a collection lens ($\Phi = 25.4$ mm, $f = 30$ mm). In this experiment, the CCD plays the role of bucket detectors, which measure only the total intensity. Compared to the single-pixel detector, the CCD has a lower noise because numbers of the readout are summed together, and it operates at a much slower rate (<50 Hz). Therefore, by using a CCD functioning as a single-pixel detector, the two thresholds scheme will perform better due to a smaller amplitude of noise, and consequently, the reconstructed image of the system will, in general, have better quality than those used an actual single-pixel detector. Random $-1/1$ binary patterns with a size of 64×64 pixels are encoded on the DMD by displaying a random 0/1 pattern and immediately succeeding it by its inverse.

When a 0/1 pattern is shown on the DMD, we sum all intensities recorded from the CCD pixels to obtain S_j^+, and, when the 0/1 pattern's inverse is shown on the DMD, we sum all of the intensities recorded from the CCD pixels to obtain S_j^-. The difference between the intensity signals that are recorded for each 0/1 pattern and
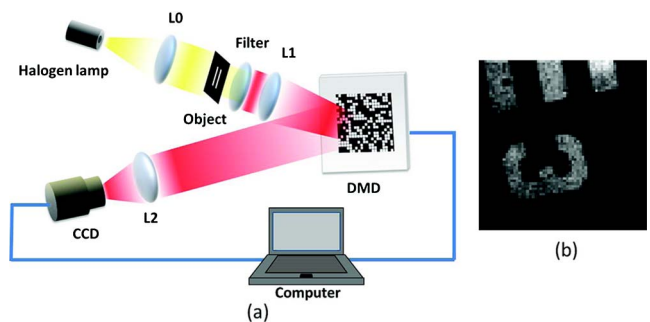
Fig. 1. (a) Schematic of CI. (b) Result reconstructed from the entire 3600 measurements. L represents lens.

its inverse (S_j^+ and S_j^-, respectively) is utilized to produce a differential signal $y_j = S_j^+ - S_j^-$, where j is the pattern number. A sequence of 3600 random $-1/1$ binary patterns is used in this experiment, and the sampling frequency is 20 Hz, which is limited by the frame rate of the CCD.

The intensity signals S_j^+ and S_j^- and random $-1/1$ binary patterns are utilized to reconstruct the image. To reconstruct the images, total variation minimization by augmented Lagrangian and alternating direction algorithms (TVAL3)[32] and the sparsity of the object gradient are utilized in this experiment. The image size is 64×64 pixels, and the result reconstructed from the entire 3600 measurements is shown in Fig. 1(b). Two thresholds T_1 and T_2 are set to reject some measurements. T_1 is employed to select the intensity measurements recorded by the bucket detector with the largest absolute values, and y_{T_1} is used to represent the measurements selected by the threshold T_1. The distribution of the $|y|$ and the threshold T_1 is shown in Fig. 2. The measurements slightly influenced by the environmental noise are selected according to T_2, and represented as y_{T_2}. y_T is the intersection between y_{T_1} and y_{T_2}. The groups of measurements determined by different thresholds and the corresponding binary patterns are used to recover the images. The values of the thresholds used will be discussed later. The results obtained by different groups of measurements are shown in Figs. 3(a)–3(f). The number of y_{T_1} and that of its complement are close, while the quality of Fig. 3(a) is considerably better than that of Fig. 3(b). The images recovered from y_{T_2} [Fig. 3(c)] and its complement [Fig. 3(d)] also show contrast. The image retrieved by y_T gives the best performance but with the least number of measurements. Compared to the background in Fig. 1(b), that in Fig. 3(e) is smoother, and the salt and pepper noise in the image have been effectively eliminated. The number of measurements required for the calculation is reduced massively by the use of these double thresholds, which is very helpful in saving computational time and storage space.

(a)　　　(c)　　　(e)

(b)　　　(d)　　　(f)
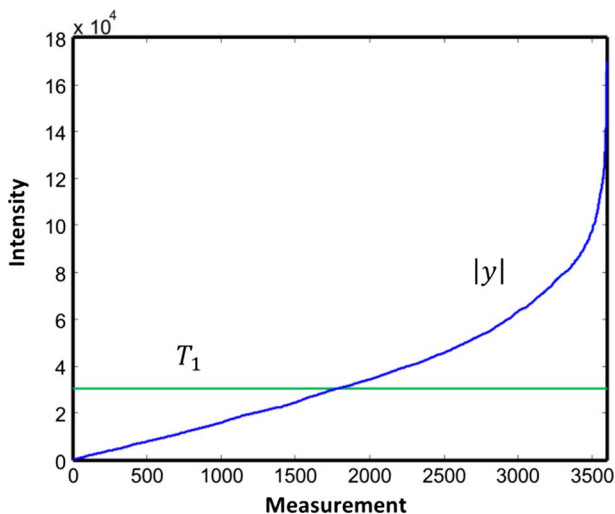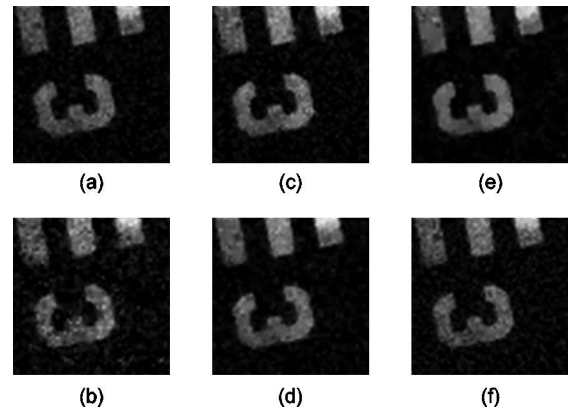
Fig. 3. Results obtained with different thresholds. (a) Image reconstructed from 1757 measurements selected by y_{T_1}, and (b) image reconstructed from the remaining 1843 measurements. (c) Image reconstructed from 1742 measurements selected by y_{T_2}, and (d) image reconstructed from remaining 1858 measurements. (e) Image reconstructed from 954 measurements selected by y_T, and (f) image reconstructed from remaining 2646 measurements.

A simulation experiment is performed to quantitatively evaluate our method. An object "CI" with a size of 64×64 pixels and a continuously varying gray scale is employed in this experiment, as shown in Fig. 4(a). The number of random $-1/1$ binary patterns is 2×10^3. The mean square error (MSE) is calculated to quantitatively characterize the reconstructed images compared to the object. The MSE is defined as

$$\mathrm{MSE} = \frac{1}{n}\sum_{i=1}^{n}\left[\hat{O}(x_i) - O(x_i)\right]^2, \qquad (8)$$

where n is the number of pixels, and i is the indices of the pixels. Naturally, the smaller the value of the MSE, the higher the quality of the recovered image is. White Gaussian noise is randomly superimposed on the intensity signals S_j^+ and S_j^- to give an SNR of $\mathrm{SNR_{signal}} = 24$ dB, where

Fig. 2. Distribution of the $|y|$ and the threshold T_1.

(a) Object

(b) MSE: 19.45
Measurement ratio: 48.8%

(c) MSE: 2.56
Measurement ratio: 8.6%

(d) MSE: 7.49
Measurement ratio: 28.1%

(e) MSE: 3.62
Measurements ratio: 14.6%
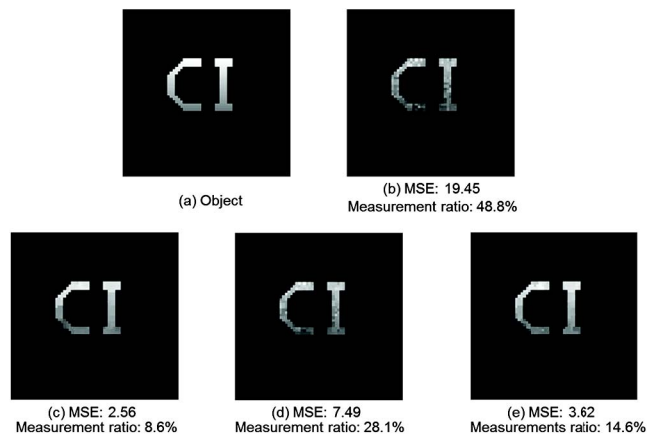
Fig. 4. (a) Object. (b) Image reconstructed from entire measurements. (c) Image reconstructed with y_T. (d) Image reconstructed with y_{T_1}. (e) Image reconstructed with y_{T_2}.

$$\mathrm{SNR_{signal}} = 20 \log\left[\frac{\sigma(\text{signal})}{\sigma(\text{noise})}\right], \qquad (9)$$

in which σ is the standard deviation. The image reconstructed from the entire 2×10^3 measurements is shown in Fig. 4(b); this image has an MSE of 19.45. The images reconstructed with y_T, y_{T_1}, and y_{T_2} are shown in Figs. 4(c)–4(e), respectively. The use of the threshold strategy provides the advantages of obtaining a better MSE and reducing the number of measurements involved in the calculation. The best qualitative image with an MSE of 2.56 is obtained by using the calculated measurements selected by the double-threshold strategy, where the number of measurements required is less than10% of the number of pixels in the object.

The quality of the reconstructed image is significantly affected by the values of the thresholds. A numerical simulation has been performed to show the relationship between the MSE and the values of the thresholds T_1 and T_2. The object is the same as the one shown in Fig. 4(a). The total number of measurements is 4×10^3. The MSEs of the images recovered from the measurements for different thresholds are calculated. The variation in the reciprocal of the MSE, according to the thresholds T_1 and T_2, is shown in Fig. 5(a). To provide a more distinct illustration, Fig. 5(b) shows the 3D intensity profile of the same image presented in Fig. 4(a). As T_1 increases and T_2 decreases, the number of measurements involved in the calculation reduces, and the quality of the recovered image improves to reach a peak after a slight deterioration. This threshold strategy is effective when a certain number of measurements are omitted. The MSE becomes minimum when $T_1 = 0.23 \max |y|$, and $T_2 = 0.25 \max |S_j - \bar{S}|$, and these two threshold values are adopted in the experiments described previously in this Letter. After reaching the peak, the reciprocal of the MSE reduces sharply. The above results indicate that omitting some measurements by setting double thresholds can enhance the image quality in CI, and the two thresholds can be determined by simulation and experimental analyses. A variety of images have been tested in the simulation experiments to determine the best values of the double thresholds. The results show that the image quality will be distinctly improved in the intervals $0.12 \max |y| < T_1 < 0.3 \max |y|$, and $0.15 \max |S_j - \bar{S}| < T_2 < 0.5 \max |S_j - \bar{S}|$, while the position of

the minimum MSE varies with different images. For the future, we will continue to theoretically and experimentally investigate the relationships between the best thresholds and the transmission ratio of the object, the statistical distributions of S_j^+ and S_j^- and the total number of measurements.

In conclusion, we present an approach that utilizes two thresholds to achieve a better MSE in CI. We select low-noise, large-fluctuation signals for the calculation. We show that by using this method image quality can be effectively improved, while saving both computational time and storage space. This threshold algorithm does not require any modifications to the existing experimental apparatus, and, therefore, the algorithm can be applied to various CI configurations. Because of these advantages, this double-threshold method is expected to be useful in practical applications.

References

1. M. F. Duarte, M. A. Davenport, D. Takhar, J. N. Laska, T. Sun, K. F. Kelly, and R. G. Baraniuk, IEEE Signal Process **25**, 83 (2008).
2. D. Donoho, IEEE Trans. Inform. Theory **52**, 1289 (2006).
3. E. Candes and M. Wakin, IEEE Signal Process **25**, 21 (2008).
4. N. Radwell, K. J. Mitchell, G. M. Gibson, M. P. Edgar, R. Bowman, and M. J. Padgett, Optica **1**, 285 (2014).
5. M. P. Edgar, Sci. Rep. **5**, 10669 (2015).
6. G. A. Howland, P. B. Dixon, and J. C. Howell, Appl. Opt. **50**, 5917 (2011).
7. G. A. Howland, D. J. Lum, M. R. Ware, and J. C. Howell, Opt. Express **21**, 23822 (2013).
8. M. J. Sun, M. P. Edgar, G. M. Gibson, B. Sun, N. Radwell, R. Lamband, and M. J. Padgett, Nat. Commun. **7**, 12010 (2016).
9. W. L. Gong, C. Q. Zhao, H. Yu, M. L. Chen, W. D. Xu, and S. S. Han, Sci. Rep. **6**, 26133 (2016).
10. V. Studer, J. Bobin, M. Chahid, H. Moussavi, E. Candes, and M. Dahan, Proc. Natl. Acad. Sci. **109**, E1679 (2012).
11. J. J. Field, D. G. Winters, and R. A. Bartels, Optica **3**, 971 (2016).
12. Y. August, C. Vachman, Y. Rivenson, and A. Stern, Appl. Opt. **52**, D46 (2013).
13. R. M. Lan, X. F. Liu, X. R. Yao, W. K. Yu, and G. J. Zhai, Opt. Commun. **366**, 349 (2016).
14. W. L. Gong and S. S. Han, Phys. Lett. A **376**, 1519 (2012).
15. J. Chen, W. L. Gong, and S. S. Han, Phys. Lett. A **377**, 1844 (2013).
16. X. R. Yao, L. Z. Li, X. F. Liu, W. K. Yu, and G. J. Zhai, Chin. Phys. B **24**, 044203 (2015).
17. W. L. Gong and S. S. Han, Sci. Rep. **5**, 9280 (2015).
18. Y. Li, Q. Li, J. Hu, and Y. Zhao, Chin. Opt. Lett. **13**, S11101 (2015).
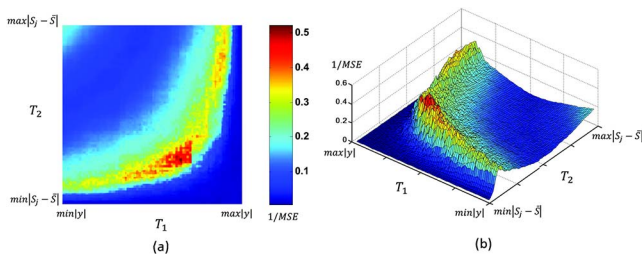
Fig. 5. (a) Reciprocal of MSE versus thresholds T_1 and T_2. (b) 3D intensity profile of image shown in (a).

19. B. Sun, M. P. Edgar, R. Bowman, L. E. Vittert, S. Welsh, A. Bowman, and M. J. Padgett, in *Computational Optical Sensing and Imaging Conference* (2013), paper CTu1C-4.

20. W. K. Yu, X. F. Liu, X. R. Yao, C. Wang, Y. Zhai, and G. J. Zhai, Sci. Rep. **4**, 5834 (2014).

21. M. J. Sun, M. P. Edgar, D. P. Phillips, G. M. Gibson, and M. J. Padgett, Opt. Express **24**, 10476 (2016).

22. L. Wang and S. M. Zhao, Photon. Res. **4**, 240 (2016).

23. Z. Zhang, X. Ma, and J. Zhong, Nat. Commun. **6**, 6225 (2015).

24. J. H. Shapiro, Phys. Rev. A **78**, 061802 (2008).

25. X. Xu, E. Li, X. Shen, and S. Han, Chin. Opt. Lett. **13**, 071101 (2015).

26. Q. Li, Z. Duan, H. Lin, S. Gao, S. Sun, and W. Liu, Chin. Opt. Lett. **14**, 111103 (2016).

27. K. H. Luo, B. Q. Huang, W. M. Zheng, and L. A. Wu, Chin. Phys. Lett. **29**, 074216 (2012).

28. M. F. Li, Y. R. Zhang, H. Fan, L. A. Wu, X. F. Liu, X. R. Yao, and K. H. Luo, Appl. Phys. Lett. **103**, 211119 (2013).

29. M. F. Li, Y. R. Zhang, K. H. Luo, L. A. Wu, and H. Fan, Phys. Rev. A **87**, 033813 (2013).

30. X. Yao, X. Liu, W. Yu, and G. Zhai, Chin. Opt. Lett. **13**, 010301 (2015).

31. C. B. Xue, X. R. Yao, X. F. Liu, G. J. Zhai, Q. Zhao, and X. Y. Guo, Opt. Commun. **393**, 118 (2017).

32. C. B. Li, "An efficient algorithm for total variation regularization with applications to the single pixel camera and compressive sensing," Master thesis (Rice University, 2010).